Materials Research. 2023; 26:e20230250
DOI: https://doi.org/10.1590/1980-5373-MR-2023-0250

Application of the Box-Behnken Design in the Optimization of Laser Powder Bed Fusion of H13 Tool Steel

Adriel P. Oliveira[1,2]*, Gustavo Figueira[1,2], Reginaldo T. Coelho[3], Claudemiro Bolfarini[1,2], Piter Gargarella[1,2,4]

[1]Universidade Federal de São Carlos, Departamento de Engenharia de Materiais, Rod. Washington Luiz, Km 235 SP-310, 13565-905, São Carlos, SP, Brasil.
[2]Universidade Federal de São Carlos, Programa de Pós-Graduação em Ciência e Engenharia de Materiais, Rod. Washington Luiz, Km 235 SP-310, 13565-905, São Carlos, SP, Brasil.
[3]Universidade de São Paulo, Escola de Engenharia de São Carlos, Departamento de Engenharia de Produção, Av. Trabalhador São-Carlense, 400, 13566-590, São Carlos, SP, Brasil.
[4]Universidade Federal de São Carlos, Centro de Caracterização e Desenvolvimento de Materiais, Rod. Washington Luiz, km 235 SP-310, 13565-905, São Carlos, SP, Brasil.

Received: May 23, 2023; Revised: July 20, 2023; Accepted: August 16, 2023

Parameter optimization is an important step in the laser powder bed fusion (L-PBF), since process defects greatly impact the mechanical properties of the final parts, especially in components that undergo cyclic loading, such as molds and dies. The present study used the H13 tool steel to show that it is possible to perform a good parameter optimization quickly and with relatively few samples. The Box-Behnken experiment design model was used along with the application of the response surface methodology. Laser power, scan speed, and hatch spacing were used as independent variables, and density and porosity were chosen as the response. Power and speed most influenced the responses, but the interaction between power and speed, and power and hatch also had a significant influence. New optimized samples showed lowest porosity, confirming the effectiveness of the model. Density can be used during parameter optimization without impairing the optimization quality.

Keywords: *Tool steel, laser powder bed fusion, additive manufacturing, optimization, Box-Behnken, response surface methodology.*

1. Introduction

Additive manufacturing (AM) has gained more and more space within the industry and is already a reality in sectors such as automotive, naval production, prostheses and implants, and aeronautics[1-3]. This technique stands out for its innovation in the production of parts with complex geometries and also for its environmental appeal since it produces less waste compared to other processes[1,4].

The mold and die industry have great potential to benefit from the advantages of AM. This is because these tools are complex and their production often involves a combination of casting, forging, and machining, which ends up causing high production time and a lot of material waste[5,6]. The H13 tool steel is one of the most used to produce molds and dies, and for this reason, it has become widely studied in the field of AM.

Among the various AM techniques currently available, laser powder bed fusion (L-PBF) has been often used. This technique allows parts to be made with fine geometric details and the construction of parts with complex internal cooling channels, which are impossible to manufacture by conventional routes, leading to a more efficient heat extraction. The higher efficiency of mold cooling allows the tool to have a longer service life and to reduce the volume of coolant fluid and overall process time[6-9].

In general, tools undergo cyclic loading and thermal stresses, so fatigue strength has a critical influence on part life. To have good fatigue resistance, the part must have as few defects as possible. Therefore, performing an adequate optimization of processing parameters is extremely important in the production of tools by AM.

Process parameter optimization needs to be performed for each set of machine and powder, so many authors performed optimization studies for H13 tool steel processed by L-PBF. Laakso et al.[10] used a D-optimal design of experiments and varied laser power and scan speed. Fonseca et al.[5] and Ren et al.[11] also varied the power and speed in different ways to find the optimal parameters without mentioning the use of any design of experiments (DOE) model. Narvan et al.[12] used a full factorial DOE model for their parameter optimization, varying laser power, scan speed, and hatch spacing. During their study, Narvan et al.[12] used the method of One Factor at a Time (OFAT) to analyze the influence of variables on the response. This method does not consider the combined influence of the parameters, only the influence of each one of them separately.

In general, the most used responses by the authors to assess the quality of the optimization are the density measured by the Archimedes method[11,13-21] or the porosity of the part calculated by optical microscopy[5,10,22-27].

*e-mail: adrielpugliesi@hotmail.com

However, using density as a response can be a problem when it comes to H13 tool steel, because this steel, when processed by L-PBF, is composed of martensite, and retained austenite, and the ratio between the two phases may vary. Since retained austenite is a denser phase, a variation in its proportion can significantly alter the density of the part, hindering a good correlation between density and porosity[21].

Furthermore, most works vary only the speed and laser power, and the optimal parameters are chosen among the analyzed options. The literature lacks systematic studies concerning the combined influence of the parameters on the responses through the response surface methodology (RSM). It is worth pointing out that other alloys, such as the 316L stainless steel, exhibit complex correlations among the L-PBF process parameters and their interactions, thus, the use of more robust statistical methods becomes imperative to deeply understand the influence of the AM process on the microstructure and properties of the H13 tool steel[28].

Considering that the optimization step is extremely important and needs to be redone when the alloy and/or the process setup is changed, the present study focused on applying the Box-Behnken (BB) DOE model to perform a robust L-PBF parameter optimization study. The model allows the response surface analysis method to be used with relatively few samples. In addition, the two responses most used in the literature (Archimedes density and porosity) were compared to assess possible differences between them.

2. Method and Materials

The present study produced samples of H13 tool steel by Laser Powder Bed Fusion (L-PBF). For this, an AM OmniSint-160 machine (OmniTek, Brazil) was used. It is equipped with Yb:YAG fiber laser with a maximum power of 400W. The H13 commercial powder used as feedstock has been previously characterized and its detailed description can be found in[21]. A total of 39 samples (10 x10 x 7 mm) were printed based on a Box-Behnken (BB) design with a triplicate of all points. This model was chosen because it allows the response surface analysis method to be used with relatively few samples. Furthermore, the BB model naturally excludes extreme combinations of parameters, which produce many defects in additive manufacturing. Figure 1 details the sample space of the Box-Behnken design.

The parameters chosen for the study were laser power, scan speed, and hatching. They are presented in Table 1. The levels of each parameter were selected based on parameters reported as optimal by works that did not consider substrate preheating, which was an unavailable feature in the machine that was employed[5,11,20,23,27,29](parameters found in the literature are summarized in Table S1 in the Supplementary material). With these data, the average and standard deviation of each selected parameter was calculated, regardless the scanning strategy employed in each specific study. The levels of each parameter were defined so that the central point was close to the mean and the lower and upper intervals were close to the standard deviation.

The scanning strategy used in this work was a unidirectional movement of the laser, performed in 5 mm strips and with a 32° rotation between layers (it is the same as described in[5]). Figure 2 displays the printed samples on the build platform.

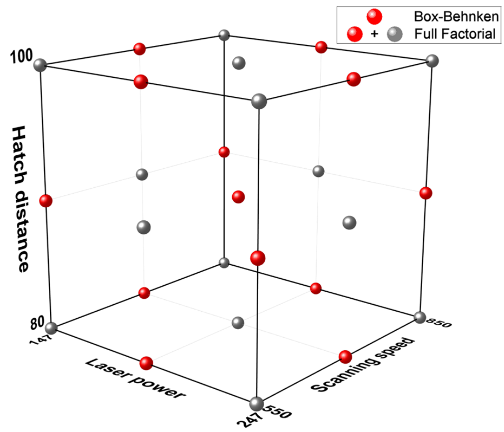

Figure 1. Sample space of the Box-Behnken design. The red dots describe experimental conditions that were evaluated, and the gray dots describe the additional conditions needed to perform a full factorial design.

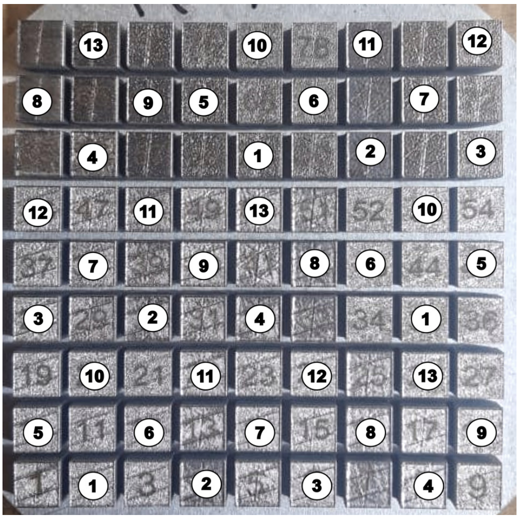

Figure 2. H13 samples produced by LPBF. The numbers inside the circles show the distribution of parameters over the substrate for optimization.

Table 1. Factors and levels used in Box-Behnken design.

Parameter	Levels		
	-1	0	1
Laser Power [W]	147	197	247
Hatch spacing [µm]	80	90	100
Scan speed [mm/s]	550	700	850

The numbers inside the circles represent the combination of parameters used for the sample (which can be seen in Table 2). The repeated numbers represent the triplicates, making it possible to know in which region of the substrate each triplicate was positioned. The unnumbered samples are additional printed samples that will not be covered in this work.

The samples had their density measured by the Archimedes method using a Gehaka DSL 910 Digital Densimeter. For the quantification of porosity, the 39 selected BB samples were longitudinally cut approximately 2mm from the right-side surface, considering the view from the outside of the machine. Subsequently, they were sanded and polished with diamond paste (3µm). Five images with 50x magnification were taken on each sample, in different regions of the polished surface. Images were acquired with an Olympus BX41M-LED optical microscope and pores were measured with pixel counts using ImageJ software. The average porosity of the five images was considered as the porosity of the sample. The two distinct responses (density and porosity) were chosen to assess whether they will present a good correlation. If the printed H13 steel has a significantly variable fraction of retained austenite between the tested parameters, it is expected that density and porosity do not correlate very well. However, if the variation of retained austenite is not significant, it is expected that density and porosity present a good correlation.

For data analysis, STATISTICA 12 software was used with a confidence level fixed at 95%. Response surfaces were obtained for density and porosity. Optimal porosity parameters were chosen to be used in making the test samples with 10 x 10 x 20 mm (Figure 3). Such samples were constructed with the reused same powder after being sieved. New density and porosity analyzes were performed and compared with previous data.

3. Results

Table 2 shows the parameters, the levels chosen, and the combinations proposed for the Box-Behnken design. The density and porosity responses corresponding to each triplicate of each combination can be seen in the final columns of the table. Those results can be graphically visualized by plotting the density and porosity as a function of volumetric energy density[2], see Figure 4. It is possible to observe that the density increases rapidly with increasing volumetric energy density (VED) until a relatively stable level.

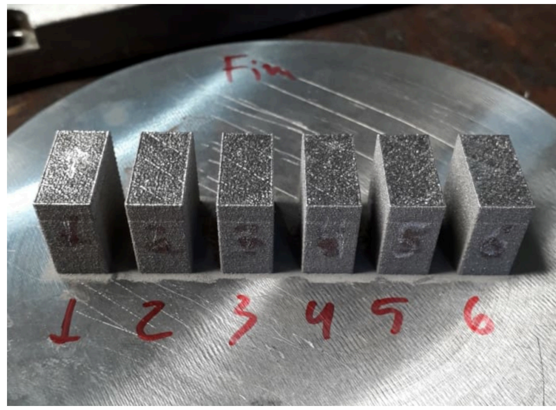

Figure 3. Samples produced later with the optimal parameters.

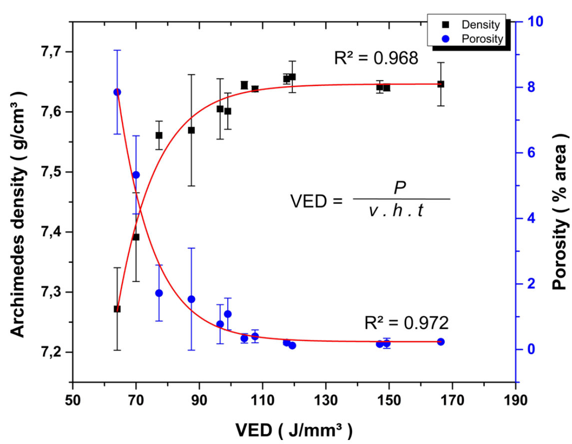

Figure 4. Density and porosity graphs of samples as a function of applied VED.

Table 2. Box-Behnken planning and results of the density and porosity responses of the samples with their real and coded values.

Exp	Power [W]	Hatch [µm]	Speed [mm/s]	Density [g/cm³]			Porosity [%]		
1	147 (-1)	80 (-1)	700 (0)	7.660	7.475	7.573	0.377	3.305	0.923
2	197 (0)	80 (-1)	550 (-1)	7.647	7.641	7.635	0.365	0.083	0.111
3	197 (0)	80 (-1)	850 (1)	7.620	7.646	7.549	0.435	0.415	1.460
4	247 (1)	80 (-1)	700 (0)	7.653	7.638	7.633	0.196	0.118	0.179
5	147 (-1)	90 (0)	550 (-1)	7.635	7.577	7.592	0.707	1.62	0.909
6	147 (-1)	90 (0)	850 (1)	7.340	7.203	7.273	6.433	8.20	8.92
7	197 (0)	90 (0)	700 (0)	7.651	7.643	7.639	0.211	0.310	0.492
8	247 (1)	90 (0)	550 (-1)	7.688	7.623	7.628	0.224	0.216	0.264
9	247 (1)	90 (0)	850 (1)	7.644	7.634	7.637	0.625	0.252	0.324
10	147 (-1)	100 (1)	700 (0)	7.470	7.323	7.381	3.993	6.285	5.707
11	197 (0)	100 (1)	550 (-1)	7.680	7.629	7.665	0.113	0.135	0.113
12	197 (0)	100 (1)	850 (1)	7.577	7.572	7.534	1.078	1.392	2.690
13	247 (1)	100 (1)	700 (0)	7.649	7.651	7.664	0.284	0.187	0.163

Porosity presents an inverse behavior. The standard deviations of each condition also decrease with increasing VED. Figure 5 shows, with OM images, how porosity varies. From images a) to d), the porosity decreases with increasing VED. From images d) to e), the porosity slightly increases again with increasing VED.

The results shown in Table 2 were submitted to the analysis of variance (ANOVA). Table 3 presents the ANOVA with the lack of fit test performed to validate the mathematical model. Since the P value for the lack of fit is less than 0.05, it is noted that the lack of fit was significant. So, the quadratic model is not perfectly adjusted to the data obtained because the mean square lack of fit (MSlof) and the mean square pure error (MSPe), which are estimates of these errors, are statistically different. Despite this, the model presented a value of 0.8754 for the R-square, which indicates a good predictive capacity. The reasons for the significant lack of fit observed will be discussed later.

In Table 3 it is also possible to see that laser power, speed, and the interaction between power and speed are the three factors that most influence the response; however, the hatch spacing and the interaction between the power and the hatch spacing also had a significant influence. Similar results were obtained considering the density as response.

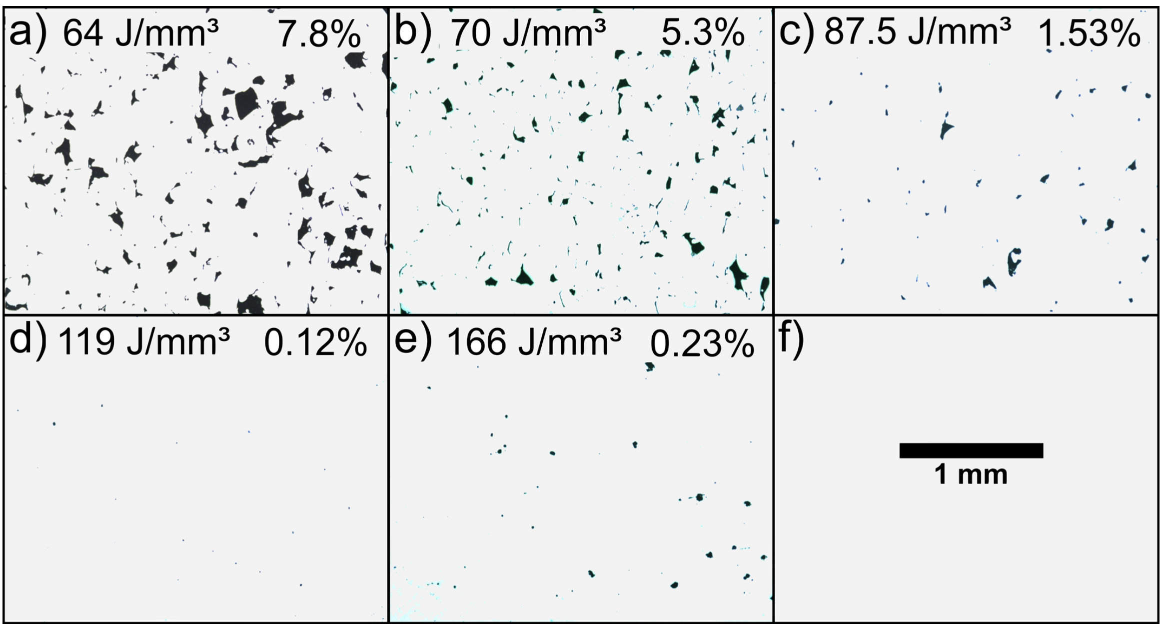

Figure 5. OM images taken from samples in different energy density ranges. The information in the images shows the VED used and the porosity calculated for each sample, respectively. All images have the same magnification, and the scale bar is presented in Figure f). The gray background was artificially added to increase the readability of the image.

Table 3. ANOVA for the porosity response (95% confidence level).

Model summary: R-sqr = 87.54%; Adj: 83.67%					
Factor	SS	df	MS	F	p
P [L]	81.9839	1	81.98393	154.6316	0.000000
P [Q]	17.1693	1	17.16931	32.3834	0.000005
h [L]	8.3700	1	8.36998	15.7868	0.000501
h [Q]	0.0836	1	0.08356	0.1576	0.694606
v [L]	31.1863	1	31.18630	58.8211	0.000000
v [Q]	1.5285	1	1.52847	2.8829	0.101465
P versus h	10.5259	1	10.52589	19.85310	0.00014
P versus v	32.7235	1	32.72348	61.72045	2.48105E-08
h versus v	0.7738	1	0.77379	1.45945	0.23789
Lack of Fit	12.9750	3	4.32499	8.15746	0.00054
Pure Error	13.7849	26	0.53019		
Total SS	214.7243	38			
Regression Equation	$1.633_{\pm 0.121} -1.848_{\pm 0.148} (P) -0.791_{\pm 0.139} (P^2) + 0.590_{\pm 0.148} (h) + 0.055_{\pm 0.139} (h^2) + 1.139_{\pm 0.148} (v) -0.236_{\pm 0.139} (v^2) -0.936_{\pm 0.210} (P \times h) -1.651_{\pm 0.210} (P \times v) + 0.253_{\pm 0.210} (h \times v)$				

P = laser power; v = scan speed; h = hatch spacing.

Figure 6 shows the marginal means. In the images, it is possible to see how each isolated parameter influences the responses. Image a) shows that the increase in power causes the density to increase abruptly up to 197W. From 197W to 247W the density continues to increase slightly. The increase in speed, seen in image b), causes the density to drop practically constantly within the analyzed points. The hatch increase, in turn, causes a decrease in density at first (from 80 μm to 90 μm), and then a slight increase (from 90μm to 100μm), but with a large standard deviation. Images d), e), and f) show that for porosity, the behavior is practically the inverse of that observed for density.

Figure 7 shows the response surfaces obtained. The surfaces allow analyzing how the interaction between parameters affects the response. For example, in image a), it is noted that, for low speeds, increasing the power raises the density only up to a certain point before the density drops again. However, at high speeds, it is noted that the increase in power makes the density only increase. Images b) and c) show the interaction of the hatch with power and speed, respectively. For these two cases, there is a processing range where the hatch can be varied without significant decreases in density. Images d), e), and f) show the response surfaces for porosity. The behavior is almost a mirror of density responses.

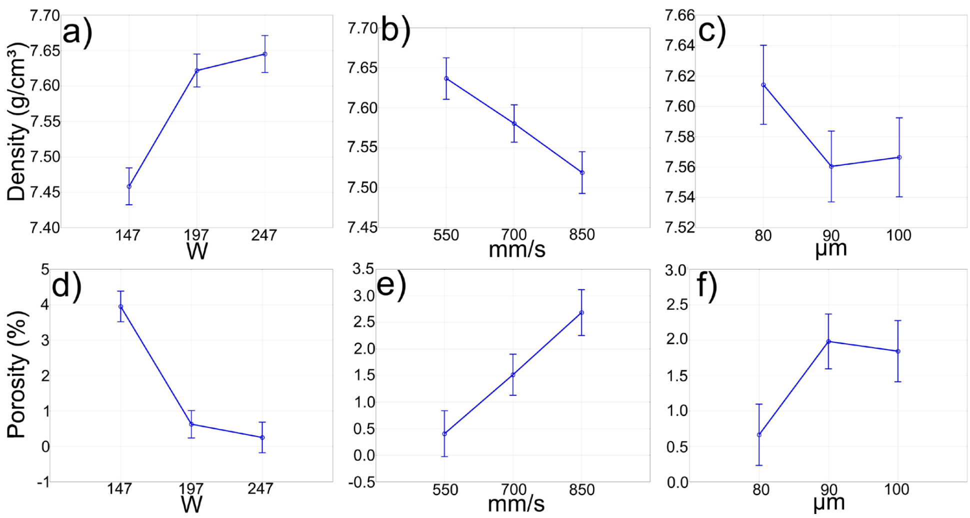

Figure 6. Marginal means obtained for the density (images a), b), and c)) and porosity (images d), e) and f)).

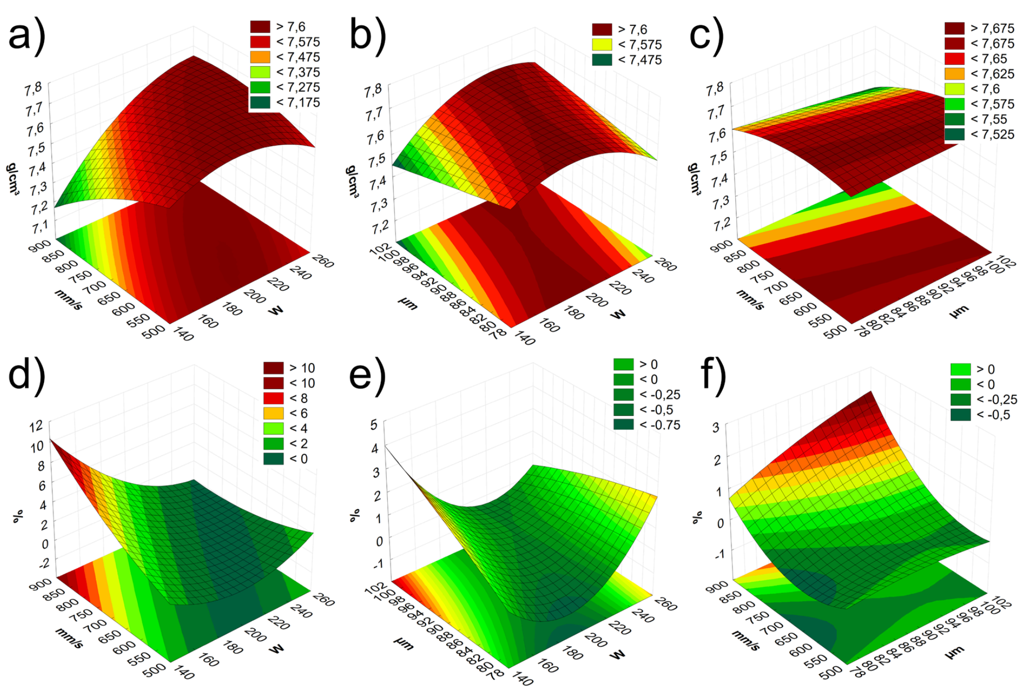

Figure 7. Response surfaces obtained for density (g/cm³) (images a), b) and c)) and porosity (%) (images d), e) and f)).

Table 4. Optimal parameters obtained for the two responses and the corresponding VED.

	Power	Scan speed	Hatch	VED
Density	211 W	586 mm/s	92 μm	130 J/mm^3
Porosity	212 W	580 mm/s	95 μm	128 J/mm^3

Table 5. Archimedes density measured in samples produced with optimal parameters.

Sample	Density (g/cm^3)
1	7.640 ± 0.005
2	7.684 ± 0.004
3	7.684 ± 0.020
4	7.688 ± 0.006
5	7.686 ± 0.006
6	7.678 ± 0.009

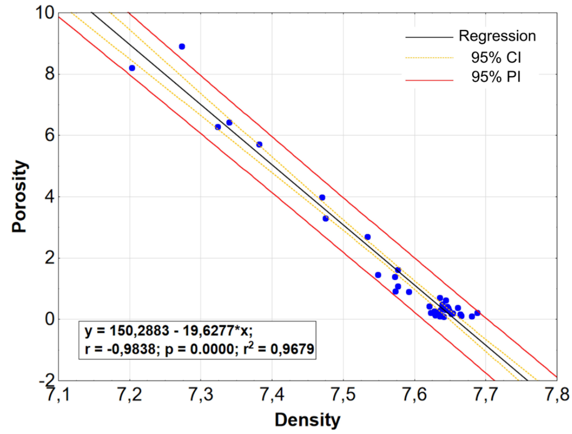

Figure 8. Correlation between density and porosity. (CI and PI represent the confidence interval and the prediction interval, respectively).

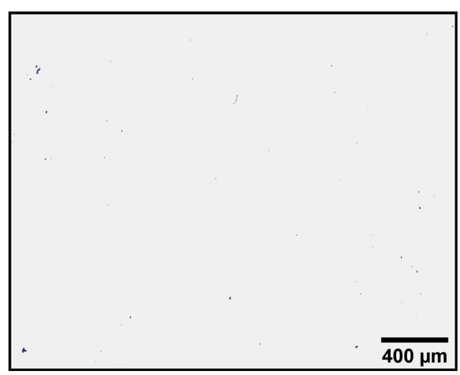

Figure 9. Image of sample 3 used to calculate porosity (0.09 ±0.03%). The gray background was artificially added to increase the readability of the image.

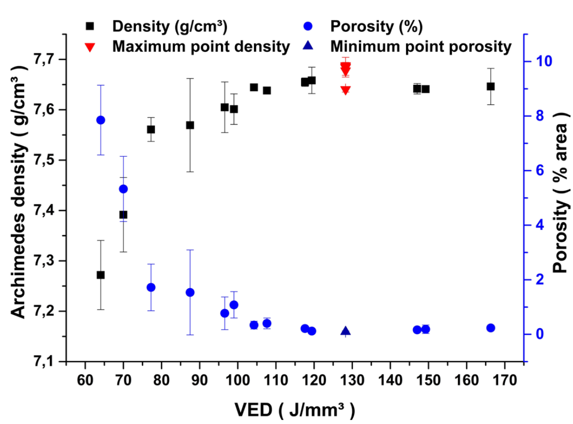

Figure 10. Density and porosity graphs as a function of applied energy density, showing the results of parts built with optimal parameters.

It is observed that in the porosity scale, there are values below zero. This is physically impossible in practice and reflects some limitations of the model that will be discussed later.

Table 4 displays the optimal parameters (maximum density and minimum porosity) calculated by the software from the model data. Note that the optimal parameters were very similar for the two responses. Figure 8 displays a correlation curve between density and porosity, made with the data from Table 2. It can be noted that the correlation between the two responses was high ($r^2 = 0.9679$).

The optimal porosity parameters were chosen to manufacture six new parts and test the validity of the model, as previously shown in Figure 3. Table 5 shows the density values for all new parts. Sample 3 was cut 2mm from the surface, sanded and polished, and then taken to the OM for porosity calculation. An image of it can be seen in Figure 9.

Figure 10 shows the curves from Figure 4 with added data from samples manufactured with the optimal parameters. It is possible to notice that both density and porosity presented better results than all other conditions analyzed. For density, only sample 1 showed a lower value than the highest value obtained previously for the mean of the triplicates (7.658g/cm^3). As for porosity, the lowest average value among the Box-Behnken triplicates was 0.12%, while the value found for the optimal condition was 0.09 ± 0.03%.

4. Discussion

This study investigated the application of the Box Behnken experimental design model in optimizing process parameters of L-PBF. The initial analysis of the produced samples showed that the density increases as the VED increases during the process. This rise occurs up to a certain point, after which the density tends to drop slightly. This has already been observed in previous studies and can be explained by the types of defects formed at each process step. Initially, at low VED, the predominant type of defect is lack of fusion (LOF). This defect has a highly irregular shape and is caused by gaps where the material has not been fused by the laser[5,10,11,13].

As the VED increases, the LOF decreases, increasing the density. However, when the VED increases too much, defects are no longer caused by lack of fusion but by the instability of the melting pool, entrapment of gases, or evaporation of alloying elements[2,5,11]. These defects can be smaller and more circular pores or larger pores caused by pool instability (Keyhole).

The model proposed for optimization showed a lack of fit, as seen in Table 3. This could have happened for two main reasons: 1) the absence of randomness in the positioning of the samples on the substrate and/or 2) a very wide experimental domain. In the first case, due to a limitation in the software of the machine used, it was not possible to distribute the samples in a truly random way. Each triplicate was distributed in a way that was far from each other. This can be a problem since the samples closer to the substrate edge tend to suffer more defects due to laser chromatic aberration when a beam with Gaussian shape is employed. Thus, the absence of a truly random distribution of the positioning of the samples may have caused the lack of fit of the model. In the second case, the distance between the levels of each variable may have facilitated the lack of fit. A broader sample space can be ineffective as several physical phenomena may occur.

Despite the lack of fit, the model showed good predictive ability. This can be assessed by the R-square values obtained for density and porosity, which were 0.861 and 0.875, respectively. Furthermore, the test samples made with the optimal parameters obtained showed better results (higher density and lower porosity) than the average values of the triplicates previously found. This shows that parameter optimization using the DOE Box-Behnken model was effective in obtaining H13 parts with minimal defects using a reduced number of samples.

The application of RSM showed that two interactions between parameters are significant. One is the interaction between laser power and scan speed and the other is the interaction between laser power and hatch. In the first case, at low power, increasing the speed causes the defects to increase severely. But at high power, increasing the speed causes a mild decrease in defects. This may be related to the geometry of the melting pool, which at high powers ends up becoming very deep and favoring the formation of Keyhole defects. However, as the speed increases, the geometry of the melting pool changes, becoming shallower and allowing for greater stability[30,31]. In the second case, when increasing the hatch at low powers, the defects increase more severely, which is related to the greater probability of the formation of lack of fusion defects. At high powers, increasing the hatch makes the defects decrease mildly. This happens because, with low hatch distance, the high level of overlapped tracks raises the temperature of the powder bed, favoring the formation of Keyhole defects. Increasing the hatch decreases overlap, allowing for better temperature distribution[30].

The application of the RSM also allowed obtaining the optimal parameters according to each response (density by Archimedes method and porosity measured by OM). The optimal parameters provided by the two responses had no significant difference. No parameter had a difference greater than 3.5%, and the VED varied by only 1.5%. Furthermore, the density and porosity data showed a high correlation index. At first glance, this correlation may seem obvious, as a higher number of defects in a part typically results in lower density. However, as demonstrated in[21], for H13 processed by L-PBF, the sample with the highest density is not always the one with the fewest defects.

A sample with a high amount of retained austenite (a denser phase) may exhibit a higher density but still have a relatively high number of defects. Conversely, a sample with a lower amount of RA may have lower density but a significantly reduced number of defects. In the cited study, the range of process parameters is significantly larger (VED between 80 and 650 J/mm^3), allowing for more significant variation in the phase fraction with the tested parameters. In the present study, the range of tested parameters is smaller (VED between 60 and 170 J/mm^3).

The high correlation between density and porosity in this study indicates that, within the range of analyzed parameters, the variation in the fraction of the constituent phases (martensite and retained austenite) is not significant. These results show that it is possible to use density as a response and still obtain a good parameter optimization quality. This is quite interesting, as the quantification of porosity by OM in all samples is significantly more laborious and time-consuming since they need to be cut, sanded, and polished.

5. Conclusion

This study investigated the application of the Box Behnken experiment design model in the optimization of laser powder bed fusion of H13 tool steel. The following conclusions are made:

- The Box Behnken model was very useful for parameter optimization, providing good results and with a smaller number of samples used concerning works previously reported in the literature.
- Analyzes of the statistical model for the two distinct responses (density by Archimedes and porosity by OM) showed very similar optimal parameter values, within the range of parameters used. These results favor the use of the Archimedes method since calculating the porosity of all samples by OM is more laborious and time-consuming.
- The interactions between the parameters were investigated, and two showed a significant impact on the responses. The interaction between laser power and scan speed, and the interaction between laser power and hatch spacing.
- For future work, reducing the range of parameter values used for optimization may improve the predictive capacity of the statistical model.

6. Acknowledgments

This study was financed in part by the Coordenação de Aperfeiçoamento de Pessoal de Nível Superior - Brazil (CAPES) - Finance Code 001. The authors would like to thank the São Paulo Research Foundation (FAPESP) for the financial support received through project nos. 2016/11309-0, 2017/27031-4, and 2018/15659-1. The authors are also grateful to Omnitek for the support with the preparation of the LPBF samples.

7. References

1. DebRoy T, Mukherjee T, Milewski JO, Elmer JW, Ribic B, Blecher JJ, et al. Scientific, technological and economic issues in metal printing and their solutions. Nat Mater. 2019;18(10):1026-32. http://dx.doi.org/10.1038/s41563-019-0408-2.
2. DebRoy T, Wei HL, Zuback JS, Mukherjee T, Elmer JW, Milewski JO, et al. Additive manufacturing of metallic components: process, structure and properties. Prog Mater Sci. 2018;92:112-224. http://dx.doi.org/10.1016/j.pmatsci.2017.10.001.
3. Herzog D, Seyda V, Wycisk E, Emmelmann C. Additive manufacturing of metals. Acta Mater. 2016;117:371-92. http://dx.doi.org/10.1016/j.actamat.2016.07.019.
4. Bajaj P, Hariharan A, Kini A, Kürnsteiner P, Raabe D, Jägle EA. Steels in additive manufacturing: a review of their microstructure and properties. Mater Sci Eng A. 2020;772:138633. http://dx.doi.org/10.1016/j.msea.2019.138633.
5. Fonseca EB, Gabriel AHG, Araújo LC, Santos PLL, Campo KN, Lopes ESN. Assessment of laser power and scan speed in fl uence on microstructural features and consolidation of AISI H13 tool steel processed by additive manufacturing. Addit Manuf. 2020;34:101250. http://dx.doi.org/10.1016/j.addma.2020.101250.
6. Mazur M, Leary M, McMillan M, Elambasseril J, Brandt M. SLM additive manufacture of H13 tool steel with conformal cooling and structural lattices. Rapid Prototyping J. 2016;22(3):504-18. http://dx.doi.org/10.1108/RPJ-06-2014-0075.
7. Mazur M, Brincat P, Leary M, Brandt M. Numerical and experimental evaluation of a conformally cooled H13 steel injection mould manufactured with selective laser melting. Int J Adv Manuf Technol. 2017;93(1-4):881-900. http://dx.doi.org/10.1007/s00170-017-0426-7.
8. Armillotta A, Baraggi R, Fasoli S. SLM tooling for die casting with conformal cooling channels. Int J Adv Manuf Technol. 2014;71(1–4):573-83. http://dx.doi.org/10.1007/s00170-013-5523-7.
9. Heogh W, Yeon SM, Kang D-S, Park S, Park S, Ryu K, et al. The design and additive manufacturing of an eco-friendly mold utilized for high productivity based on conformal cooling optimization. Mater Des. 2022;222:111088. http://dx.doi.org/10.1016/j.matdes.2022.111088.
10. Laakso P, Riipinen T, Laukkanen A, Andersson T, Jokinen A, Revuelta A, et al. Optimization and simulation of SLM process for high density H13 tool steel parts. Phys Procedia. 2016;83:26-35. http://dx.doi.org/10.1016/j.phpro.2016.08.004.
11. Ren B, Lu D, Zhou R, Li Z, Guan J. Preparation and mechanical properties of selective laser melted H13 steel. J Mater Res. 2019;34(8):1415-25. http://dx.doi.org/10.1557/jmr.2019.10.
12. Narvan M, Al-Rubaie KS, Elbestawi M. Process-structure-property relationships of AISI H13 tool steel processed with selective laser melting. Materials. 2019;12(14):2284. http://dx.doi.org/10.3390/ma12142284.
13. Yonehara M, Ikeshoji TT, Nagahama T, Mizoguchi T, Tano M, Yoshimi T, et al. Parameter optimization of the high-power laser powder bed fusion process for H13 tool steel. Int J Adv Manuf Technol. 2020;110(1–2):427-37. http://dx.doi.org/10.1007/s00170-020-05879-6.
14. Yan J, Song H, Dong Y, Quach WM, Yan M. High strength (~2000 MPa) or highly ductile (~11%) additively manufactured H13 by tempering at different conditions. Mater Sci Eng A. 2020;773:138845. http://dx.doi.org/10.1016/j.msea.2019.138845.
15. Deirmina F, Peghini N, AlMangour B, Grzesiak D, Pellizzari M. Heat treatment and properties of a hot work tool steel fabricated by additive manufacturing. Mater Sci Eng A. 2019;753:109-21. http://dx.doi.org/10.1016/j.msea.2019.03.027.
16. Pellizzari M, Furlani S, Deirmina F, Siriki R, AlMangour B, Grzesiak D. Fracture toughness of a hot work tool steel fabricated by laser-powder bed fusion additive manufacturing. Steel Res Int. 2020;91(5):1900449. http://dx.doi.org/10.1002/srin.201900449.
17. Narvan M, Ghasemi A, Fereiduni E, Kendrish S, Elbestawi M. Part deflection and residual stresses in laser powder bed fusion of H13 tool steel. Mater Des. 2021;204:109659. http://dx.doi.org/10.1016/j.matdes.2021.109659.
18. Lei F, Wen T, Yang F, Wang J, Fu J, Yang H, et al. Microstructures and mechanical properties of H13 tool steel fabricated by selective laser melting. Materials. 2022;15(7):2686. http://dx.doi.org/10.3390/ma15072686.
19. Miyauchi H, Matsumoto H, Yokota K. Selective laser melting with changing input energy periodically for production of partially hardened laminate structure in H13 steel. J Manuf Process. 2022;73:839-48. http://dx.doi.org/10.1016/j.jmapro.2021.11.028.
20. Wang M, Li W, Wu Y, Li S, Cai C, Wen S, et al. High-temperature properties and microstructural stability of the AISI H13 Hot-work tool steel processed by selective laser melting. Metall Mater Trans, B, Process Metall Mater Proc Sci. 2019;50(1):531-42. http://dx.doi.org/10.1007/s11663-018-1442-1.
21. Oliveira AP, Lima LHQR, Felipe BC, Bolfarini C, Coelho RT, Gargarella P. Effect of microstructure and defect formation on the bending properties of additive manufactured H13 tool steel. J Mater Res Technol. 2021;15:3598-609. http://dx.doi.org/10.1016/j.jmrt.2021.10.011.
22. Dzukey GA, Yang K, Wang Q, Zhuang B, Hou W. Porosity, hardness, friction and wear performance analysis of H13 SLM-formed samples. J Mater Eng Perform. 2020;29(8):4957-66. http://dx.doi.org/10.1007/s11665-020-04999-0.
23. Lee J, Choe J, Park J, Yu JH, Kim S, Jung ID, et al. Microstructural effects on the tensile and fracture behavior of selective laser melted H13 tool steel under varying conditions. Mater Charact. 2019;155:109817. http://dx.doi.org/10.1016/j.matchar.2019.109817.
24. Savrai RA, Toporova DV, Bykova TM. Improving the quality of AISI H13 tool steel produced by selective laser melting. Opt Laser Technol. 2022;152:108128. http://dx.doi.org/10.1016/j.optlastec.2022.108128.
25. Qin S, Bo Y, Herzog S, Hallstedt B, Kaletsch A, Broeckmann C. Influence of process parameters on porosity and hot cracking of AISI H13 fabricated by laser powder bed fusion. Powders. 2022;1(3):184-93. http://dx.doi.org/10.3390/powders1030012.
26. Sun Y, Wang J, Li M, Wang Y, Li C, Dai T, et al. Thermal and mechanical properties of selective laser melted and heat treated H13 hot work tool steel. Mater Des. 2022;224:111295. http://dx.doi.org/10.1016/j.matdes.2022.111295.
27. Mertens R, Vrancken B, Holmstock N, Kinds Y, Kruth J-P, Van Humbeeck J. Influence of Powder Bed Preheating on Microstructure and Mechanical Properties of H13 Tool Steel SLM Parts. Phys Procedia. 2016;83:882-90. http://dx.doi.org/10.1016/j.phpro.2016.08.092.
28. Miranda G, Faria S, Bartolomeu F, Pinto E, Madeira S, Mateus A, et al. Predictive models for physical and mechanical properties of 316L stainless steel produced by selective laser melting. Mater Sci Eng A. 2016;657:43-56. http://dx.doi.org/10.1016/j.msea.2016.01.028.
29. Ackermann M, Šafka J, Voleský L, Bobek J, Kondapally JR. Impact testing of H13 tool steel processed with use of selective laser melting technology. Mater Sci Forum. 2018;919:43-51. http://dx.doi.org/10.4028/www.scientific.net/MSF.919.43.
30. Khairallah SA, Anderson AT, Rubenchik A, King WE. Laser powder-bed fusion additive manufacturing: physics of complex melt flow and formation mechanisms of pores, spatter, and denudation zones. Acta Mater. 2016;108:36-45. http://dx.doi.org/10.1016/j.actamat.2016.02.014.
31. Khairallah SA, Martin AA, Lee JRI, Guss G, Calta NP, Hammons JA, et al. Controlling interdependent meso-nanosecond dynamics and defect generation in metal 3D printing. Science. 2020;368(6491):660-5. http://dx.doi.org/10.1126/science.aay7830.

Supplementary material

The following online material is available for this article:

Table S1 – L-PBF process parameters used for H13 tool steel in several works in the literature.